The determination of the activation energy for a Vibro-impact system under multiple excitations

jianlong wang (jlwang@nuaa.edu.cn)
Nanjing University of Aeronautics and Astronautics College of Aerospace Engineering
https://orcid.org/0000-0001-8068-6468

Xiaolei Leng
Nanjing University of Aeronautics and Astronautics

Xianbin Liu
Nanjing University of Aeronautics and Astronautics

Research Article

Keywords: Vibro impact system, activation energy, large deviation theory , mean first exit time, the most probable exit path

Posted Date: March 30th, 2021

DOI: https://doi.org/10.21203/rs.3.rs-272833/v1

The determination of the activation energy for a Vibro-impact system under multiple excitations

Jianlong Wang, Xiaolei Leng*, Xianbin Liu

State Key Laboratory of Mechanics and Control of Mechanical Structure, Nanjing University of Aeronautics and Astronautics

*Corresponding author, email: lengxl@nuaa.edu.cn

Abstract

In this paper, the stochastic stability of a Vibro-impact system with multiple excitation forces is studied. Due to the multiple external excitations, the probability density function (PDF) of the system is extremely difficult to solve. In addition, the existence of coexisting steady states is very common for the Vibro-impact system, and the perturbation of random noise will cause the transitions between the steady states. In this case, we are more interested in working out each attractor's activation energy, which is specifically used to characterize the attractor's stochastic stability, rather than the solution of the PDF. Based on the large deviation theory, the asymptotic analysis is carried out, and a time-varying Hamilton's equation for the quasi-potential is derived. To verify the effectiveness of the theoretical analysis, two detailed examples, where an impact attractor and a non-impactor coexist in the system, are conducted. By the application of the action plot method, the activation energies and the most probable exit paths (MPEP) for each attractor are derived. Compared with the numerical simulation, it shows very good agreement. Moreover, it is found that the existence of transient chaos near the attractor could seriously deteriorate the attractor's stability.

Keywords: Vibro-impact system, activation energy, large deviation theory, mean first exit time, the most probable exit path

1. Introduction

Vibro-impact systems are usually of many engineering applications, such as vibratory pile drivers, pie placers, heat exchange tubes in nuclear reactors [1]. Because of its importance in the industry, many studies concerning the Vibro-impact system's dynamical mechanisms have been made during the past decades. For the deterministic aspect, those studies mainly focus on the modeling of the Vibro-impact system, analyzing the bifurcation and the chaotic behavior, and studying the local stability [2–8]. For the stochastic aspect, because the PDF is very useful for us to analyze the stochastic system's stability, the researchers are dedicated to solving the response PDFs of the Vibro-impact system under various random excitations [9–18]. For example, Fen et al. have studied the Vibro-impact Duffing oscillator's stationary responses excited by additive Gaussian white noise by using the quasi-conservative averaging method [13]. Zhu obtained the stationary PDFs of the Vibro-impact Duffing system under external Poisson impulses with the exponential–polynomial closure method [12]. And Dimentberg derived a closed-form solution for the stationary PDF of a single-mass Vibro-impact system to random white noise by the quasi-conservative approximation [11]. However, the solution of the stationary PDF is usually very difficult for stochastic systems; sometimes, it even does not exist.

In engineering, we often coincide with such a situation that a machine that runs smoothly suddenly becomes noisy; after a while, it again runs smoothly, the motion state is alternatively between smoothy and noisy, and there are no changes in the system's parameters in the whole procedure. This is usually the case that the noise induces transitions between the steady non-impact and steady-impact states. For the Vibro-impact system, the existence of coexisting steady states is very common, and the unavoidable disturbance of random noise will cause the transitions between the steady states[19–22].In this case, we are more interested in investigating the activation energy, quasi-potential, mean first exit time(MFET) of the attractors of the Vibro-impact system, rather than the solution of the stationary PDF as usually many works do [23–25]. However, so far, there are very scarce researches working on the stochastic stability of the Vibro-impact system[26,27].

In this paper, the stochastic stability of a Vibro-impact system with Hertz contact force is studied. First, in section 2, the model of the Vibro-impact system is given. In section 3, based on the large deviation theory, the asymptotic analysis for the Vibro-impact system under weak noise is carried out and obtained a time-varying Hamiltonian equation. At those parameters, where the system has multiple coexisting attractors in the state space, we perturb the system with weak random noise. Moreover, by the action plot method [28], each attractor's activation energy and MPEPs are derived. In section 4, the numerical simulation is carried out, and the theoretical results are verified. At last, conclusions are drawn in section 5.

2. The Vibro-impact system

Vibro-impact systems are encountered in many engineering applications such as structures and machines with rigid barriers, clearance, and gaps; Therefore, it is essential to study the dynamics of the Vibro-impact system. Here we consider a Vibro-impact system, which is a generic mechanical system with a clearance type nonlinearity, as shown in Fig.1, and the motion of the system obeys the equation as follows

$$\ddot{x} + 2\zeta\omega_n\dot{x} + \omega_n^2 x = F(x) + f_0\cos(\omega t) + f_1 . \tag{1}$$

where ω_n is the natural frequency, ζ is the damping coefficient. f_0 and ω are the amplitude and the frequency of the harmonic excitation, respectively. f_1 is the constant excitation, and $F(x)$ is the collision force. Systems governed by equations of this type have been studied extensively- theoretically, experimentally, and numerically[29–33].

In this paper, different from the paper[34], where the collision force is linear, we assume the collision force is governed by the Hertz contact law [35]. Thus

$$F = \begin{cases} -k_r(x-b_r)^{3/2} & x > b_r \\ 0 & -b_l < x < b_r \\ -k_l(x+b_l)^{3/2} & x < -b_l \end{cases} . \tag{2}$$

here, b_l and b_r are the left and right distances from barriers, respectively; k_l and k_r are the left and right contact stiffnesses, which are functions of geometries and material properties of mass and its both side constraints. A detailed description of the contact stiffness can be found in the paper[36].

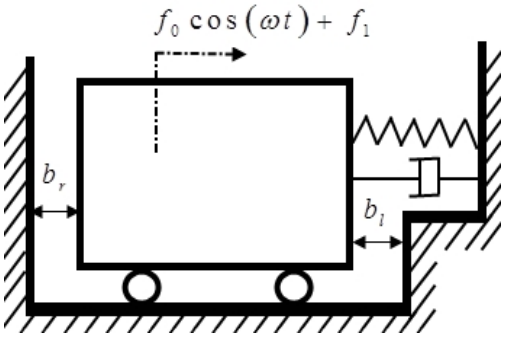

Fig.1 Schematic model of Vibro-impact oscillator

For convenience, we rewrite the system (1) as follows

$$\begin{cases} \dot{x} = y \\ \dot{y} = -\omega_n{}^2 x - 2\zeta\omega_n y + F(x) + f_0 \cos(\omega t) + f_1 \end{cases}. \tag{3}$$

The paper[27,37] shows when the damping coefficient ζ is low, the existence of multiple coexisting steady states will be a predominant feature for the system.

3. Noise Perturbed System

In a real working environment, the perturbation of the noise is always unavoidable. As we have seen, for our deterministic system, the existence of multiple coexistence steady states is a predominant feature. If the system is perturbed by random noise, the noise will induce transitions between the attractors. Hence, it is very necessary to study each attractor's stability. Traditionally, efforts are made to obtain the Stationary PDF of the system's response process. However, for our system, due to the existence of multiple coexisting stable states and multiple excitations, the solution of the FPK equation is extremely difficult. Furthermore, even the PDFs are obtained, it still could not depict the stability of the attractors well. Therefore, it is very important to determine the activation energy, quasi-potential, or the MFET of each attractor in this case. We review from large deviation theory that the asymptotic analysis for our system's response in weak noise limit is carried out, and the activation energy and the most probable transition path for each attractor are obtained theoretically[25].

3.1 Theoretical Analysis

Motions of the randomly perturbed system are usually governed by stochastic differential equations of the type

$$d\mathrm{x} = \mathrm{b}(\mathrm{x})dt + \varepsilon^{1/2}\sigma(\mathrm{x})d\mathrm{W}(t). \tag{4}$$

here x is an n-dimensional random process, ε is a small parameter used to characterize the noise's weakness, $\sigma(\mathrm{x})$ is a matrix with n rows and m columns, and $\mathrm{W}(t)$ stands for an m-dimensional standard Wiener process.

If the stationary probability density p is assumed to exist, then p is governed by the stationary FPK equation

$$-\frac{\partial}{\partial x_i}(b_i p) + \frac{\varepsilon}{2}\frac{\partial^2}{\partial x_i \partial x_j}(a_{ij} p) = 0. \tag{5}$$

where b_i is the i th coefficient of the n -dimensional drift vector $\mathrm{b}(\mathrm{x})$, a_{ij} is the ij th element of the diffusion matrix $\sigma(\mathrm{x})\sigma(\mathrm{x})^T$.

As $\varepsilon \to 0$, the quasi-potential Ψ associated with the stationary probability density p can be shown to be given by[38]:

$$\Psi(\mathrm{x}) = -\lim_{\varepsilon \to 0} \varepsilon \ln p(\mathrm{x}). \tag{6}$$

If the unperturbed system $\dot{\mathrm{x}} = \mathrm{b}(\mathrm{x})$ has only a unique attractor A, then the quasi-potential Ψ should be

$$\Psi(\mathrm{x}) = \min_{\substack{\tilde{\mathrm{x}}(T_1)=\mathrm{x}_0 \in \mathrm{A} \\ \tilde{\mathrm{x}}(T_2)=\mathrm{x}}} S_{T_1 T_2}(\tilde{\mathrm{x}}) + C(\mathrm{A}). \tag{7}$$

$C(\mathrm{A})$ is an arbitrary constant. $S_{T_1 T_2}(\tilde{\mathrm{x}})$ is the action functional of fluctuation along with the trajectory $\tilde{\mathrm{x}}$, defined by

$$S_{T_1 T_2}(\tilde{\mathrm{x}}) = \int_{T_1}^{T_2} L(\tilde{\mathrm{x}}, \dot{\tilde{\mathrm{x}}})\, dt,\ L(\tilde{\mathrm{x}}, \dot{\tilde{\mathrm{x}}}) = \frac{1}{2}\left(\dot{\tilde{\mathrm{x}}} - \mathrm{b}(\tilde{\mathrm{x}})\right)^T a^{-1}\left(\dot{\tilde{\mathrm{x}}} - \mathrm{b}(\tilde{\mathrm{x}})\right). \tag{8}$$

This has a form of Lagrangian L for a classic mechanical system.

In the case of multiple attractors A_i coexisting in the deterministic system, a global potential can be constructed by taking the minimum of all local pieces Ψ_i at each point x:

$$\Psi(\mathrm{x}) = \min_{\mathrm{A}_i} \Psi_i(\mathrm{x}). \tag{9}$$

and the constant $C(\mathrm{A}_i)$ should be appropriately adjusted relative to each other before the minimum is evaluated.

The minimization in Eq.(7) is taken over all paths $\tilde{\mathrm{x}}$, starting from any point in the attractor A and ending at a point x. The endpoints T_1 and T_2 are left free. Actually, the minimum only is achieved for the paths $\tilde{\mathrm{x}}$ taken over infinite time intervals such that $\tilde{\mathrm{x}}(-\infty) \in \mathrm{A}$ and $\tilde{\mathrm{x}}(T) = \mathrm{x}$, and they correspond to the most probable path of Eq.(4) that fluctuating from the attractor A to point x. By the method of steepest descents, several extreme paths correspond to $\delta S / \delta \tilde{\mathrm{x}} = 0$ can be derived, and the least of the action of the extreme paths corresponds to the minimum in Eq.(7). This leads to the Euler-Lagrange equation for the extreme paths, a n second-order non-linear partial differential equation given by

$$\frac{\partial L}{\partial x_i} - \frac{d}{dt}\frac{\partial L}{\partial \dot{x}_i} = 0. \tag{10}$$

However, the Euler-Lagrange equation (10) is complicated to be solved and usually is transformed into the Hamiltonian equation by using the Lagrangian. By introducing a generalized coordinate vector, q spanning an n -dimensional space with components $\{q_1, ..., q_n\}$ such that

$$q_i = x_i, \tag{11}$$

A Hamiltonian structure can be constructed:

$$H(q,p)=\sum_{i=1}^{n}p_i\dot{q}_i-L(q,\dot{q})\cdot \tag{12}$$

here the generalized momentum p_i is defined by

$$p_i\equiv\frac{\partial L}{\partial\dot{q}_i},i=1,...,n\cdot \tag{13}$$

Using Eq.(13) to solve for $\dot{q}$ as a function of p, then substituting the result for $\dot{q}$ into Eq.(12), resulting in a function depending only on q,p. Differentiating Eq. (13) with respect to time and using Eq.(10) gives

$$\dot{p}_i=\frac{\partial L}{\partial q_i}\cdot \tag{14}$$

this immediately leads to the Hamilton's equation, and the extreme paths governed by Eq.(10) can be thus found by solving the $2n$ first-order differential equations:

$$\begin{cases}\dot{q}_i=\dfrac{\partial H}{\partial p_i}\\ \dot{p}_i=-\dfrac{\partial H}{\partial q_i}\end{cases}\cdot \tag{15}$$

Supposing our system (3) is perturbed by an additive white Gaussian noise, and the motion of the system follows as

$$\begin{cases}\dot{x}=y\\ \dot{y}=-\omega_n{}^2x-2\zeta\omega_n y+F(x)+f_0\cos(\omega t)+f_1+\xi(t)\end{cases}\cdot \tag{16}$$

here the random process $\xi(t)$ has a zero mean, and an autocorrelation function $\langle\xi(t)\xi(t+\tau)\rangle=D\delta(\tau)$, D is the intensity of the noise.

Rewritten the system (16) as type (4) follows:

$$\begin{cases}dx_1=x_2dt\\ dx_2=\left(-\omega_n{}^2x_1-2\zeta\omega_n x_2+F(x_1)+f_0\cos(\omega t)+f_1\right)dt+\sqrt{D}dW(t)\end{cases}\cdot \tag{17}$$

For the drift coefficient in system (17) is periodic with respect to time t, the stationary probability density $p(\mathrm{x},t)$ assumed to exist should also be periodic for time t, so as the associated quasi-potential $\Psi(\mathrm{x},t)$. For the system is excited by a periodic excitation, we fix our study on the Poincare section plane Σ_{t_0}.

$\Sigma_{t_0}=\left\{(x,y,t)\middle|t=t_0,\mathrm{mod}(2\pi/\omega)\right\}$, which $t_0=0$ is chosen

Hence, the action functional in Eq.(8) should be changed into the form:

$$S_{T_1T_2}(\mathrm{x},t_0)=\int_{t_0+N_1T}^{t_0+N_2T}L(\mathrm{x},\dot{\mathrm{x}},s)ds\cdot \tag{18}$$

here $T=2\pi/\omega$, and the integer N_1 and N_2 are left free.

Furthermore, due to the diffusion matrix (a_{ij}) in our system is singular, the Lagrangian L should be

reformed according to the paper[39] : $L(\mathrm{x},\dot{\mathrm{x}},t)=\frac{1}{2}\left[\dot{x}_2-\left(-\omega_n^2 x_1-2\zeta\omega_n x_2+F(x_1)+f_0\cos(\omega t)+f_1\right)\right]^2$.

Appling the coordinates transformation Eq.(11), the Lagrangian L would be rewritten into the generalized coordinate, and replacing it into Eq.(13) obtains:

$$\begin{cases} p_1=2\zeta\omega_n\left[\dot{q}_2-\left(-\omega_n{}^2 q_1-2\zeta\omega_n q_2+F(q_1)+f_0\cos(\omega t)+f_1\right)\right] \\ p_2=\dot{q}_2-\left(-\omega_n{}^2 q_1-2\zeta\omega_n q_2+F(q_1)+f_0\cos(\omega t)+f_1\right) \end{cases}. \tag{19}$$

Hence the Hamiltonian for (17) is found to be

$$H=\frac{1}{2}p_2^2+p_1q_2+\left(-\omega_n{}^2 q_1-2\zeta\omega_n q_2+F(q_1)+f_0\cos(\omega t)+f_1\right)p_2. \tag{20}$$

The extreme path is then the solution of Hamilton's equations(Freidlin equation)

$$\begin{aligned} \dot{q}_1&=q_2 \\ \dot{q}_2&=\left(-\omega_n{}^2 q_1-2\zeta\omega_n q_2+F(q_1)+f_0\cos(\omega t)+f_1\right)+p_2 \\ \dot{p}_1&=\left(\omega_n{}^2-F'(q_1)\right)p_2 \\ \dot{p}_2&=-p_1+2\zeta\omega_n p_2 \end{aligned}. \tag{21}$$

and the corresponding action of the extreme path is given by

$$\dot{S}=\frac{1}{2}p_2^2. \tag{22}$$

3.2 Examples

Now, we applied the above analysis to concrete examples. We set the parameters of the system as follows[34]

$$\zeta=0.01,\quad \omega_n=1,\quad f_0=0.18,\quad f_1=0.2. \tag{23}$$

and the parameters in the contact force $F(x)$ as[35]

$$b_l=b_r=0.5, k_l=k_r=50. \tag{24}$$

Under these parameters, the system will exhibit rich phenomena. Varying the force-frequency ω, we find when $\omega=0.525$ and $\omega=0.57$, the systems exist two coexisting stable states, one is an impact attractor, and another is a non-impactor attractor. Through the GCM method[40], the global structures of the deterministic systems are shown in Fig.2. And the phase projections of the steady states are shown in Fig.3. We use attractor I to denote the steady impact state and attractor N, the non-impact steady-state, for brevity. We can see the basins of the attractor N and attractor I are separated by the stable invariant manifolds of the saddle point, and the attraction basin of attractor I is larger than that of attractor N in both cases. Hence it would be estimated that the attractor N should be less stable than attractor I for both cases. Also, we observed that the attraction basin of attractor N in $\omega=0.525$ is slightly larger than in $\omega=0.57$, so attractor N of $\omega=0.525$ should be expected to be more stable than attractor N of $\omega=0.57$, and inverse for attractor I.

Applying the action plot method [28] to Hamilton's equation (21), trajectories initialed from points (100000 points) on a small circle (radius=0.000001) centered at each of the attractors are tracked until their first exit from the attraction domain. Then the actions of the sets of the trajectories are parameterized according to the angular position, and the trajectory with the minimum action is

considered to be the most probable exit path. The MPEPs escaping from attractor I to attractor N and in revise found by the action plot are plotted on the Poincare section, as in Fig.4. Moreover, the time histories of the momentum p_2 and the action s are shown in Fig.5.

From Fig.4 and Fig.5, we can see the derived MPEPs of the attractor N spiral out from the basin of attraction until hit exactly near the saddle point, and the momentums p_2 fall nearly to zero, in full agreement with the large deviation theory. For attractor I, although the trajectory with the minimum action does not hit on the saddle point so exactly and its momentum p_2 does not drop to zero, here, we still view it as the MPEP for it is usually very near to the theoretic MPEP. In addition, from Fig.5, we can see the farther the MPEP leaves away from the attractor, the much larger the momentum p_2 is, and much more action is required. That is why the size of the basin of attraction or the distance between the attractor and the saddle point on the boundary is usually expected as a criticism to the stability of the metastable state[41,42].

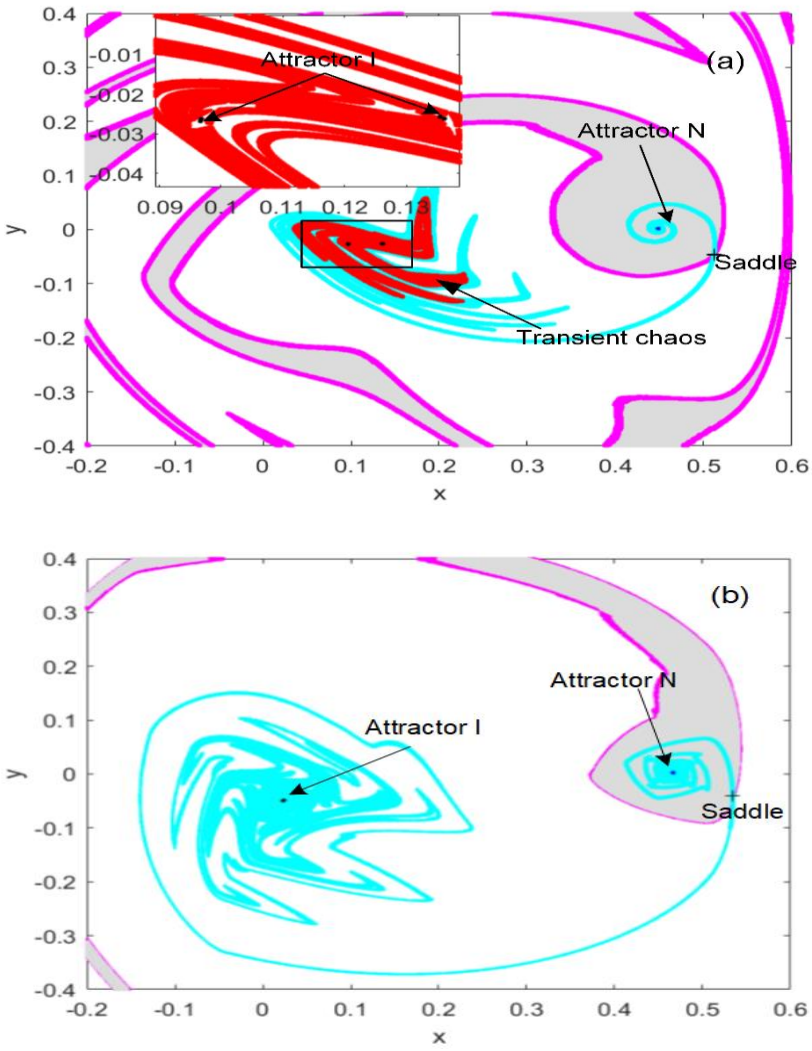

Fig.2 The Vibro-impact system's global structure on the Poincare section: attractors, semi-attractors, stable and unstable manifolds of the semi-attractors. (a) $\omega = 0.525$,(b) $\omega = 0.570$

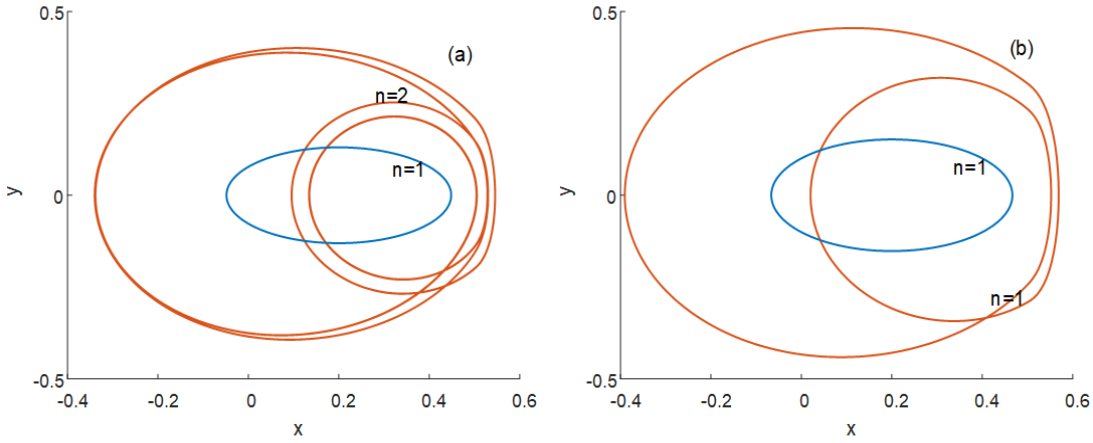

Fig.3 The steady-state phase projection: (a) $\omega = 0.525$: a steady periodic two impact orbit coexists with a periodic one non-impact orbit. (b) $\omega = 0.570$: a steady periodic one impact orbit, a steady periodic one non-impact orbit.

For $\omega = 0.525$, the corresponding activation energies for attractor I and attractor N are 0.000102 and 0.000097, respectively. For $\omega = 0.570$, the corresponding activation energies are 0.00107 and 0.000082 for attractor I and attractor N, respectively. It is consistent with our expectation that attractor N's stability should be recessed because the size of the attraction basin of attractor N decreases as the frequency increases. However, we have noted that the stabilities of attractor I differ very far for both the parameters. That is mainly attributed to the transient chaos existing in $\omega = 0.525$, which seriously deteriorates the attractor I's stability. In the transient chaos, there is a dense obit that can carry the particle to any point in the transient chaos without any external forces. Moreover, due to the quasi-potential is Lipschitz continuous[25], hence in the transient chaos, the quasi-potential is an equipotential set (as seen in Fig.5(b), the costed action is very tiny before the MPEP leaves the transient chaos). This will largely decay the attractor's active attraction basin and make the attractor much closer to the saddle point, resulting in the attractor being very unstable.

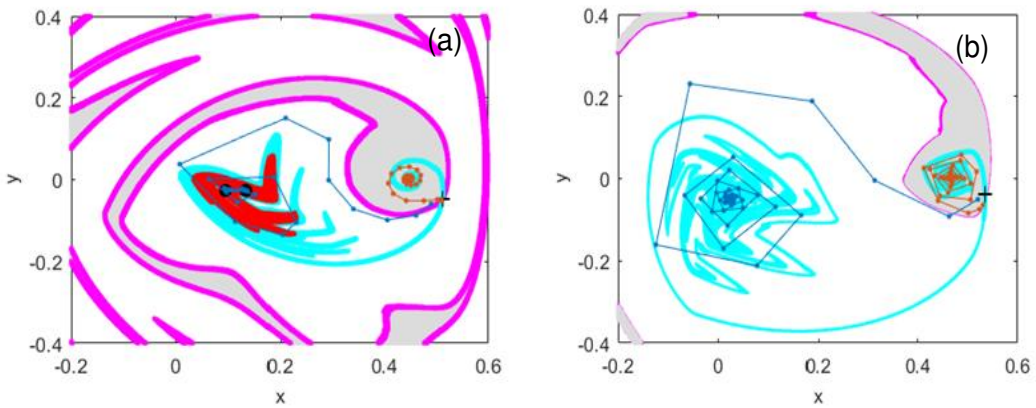

Fig.4 The MPEPs derived by the action plot. The dark blue dash lines are the most probable exit paths exiting from attractor I, and the brown ones are the most probable exit paths exiting from attractor N. (a) $\omega = 0.525$,(b) $\omega = 0.57$.

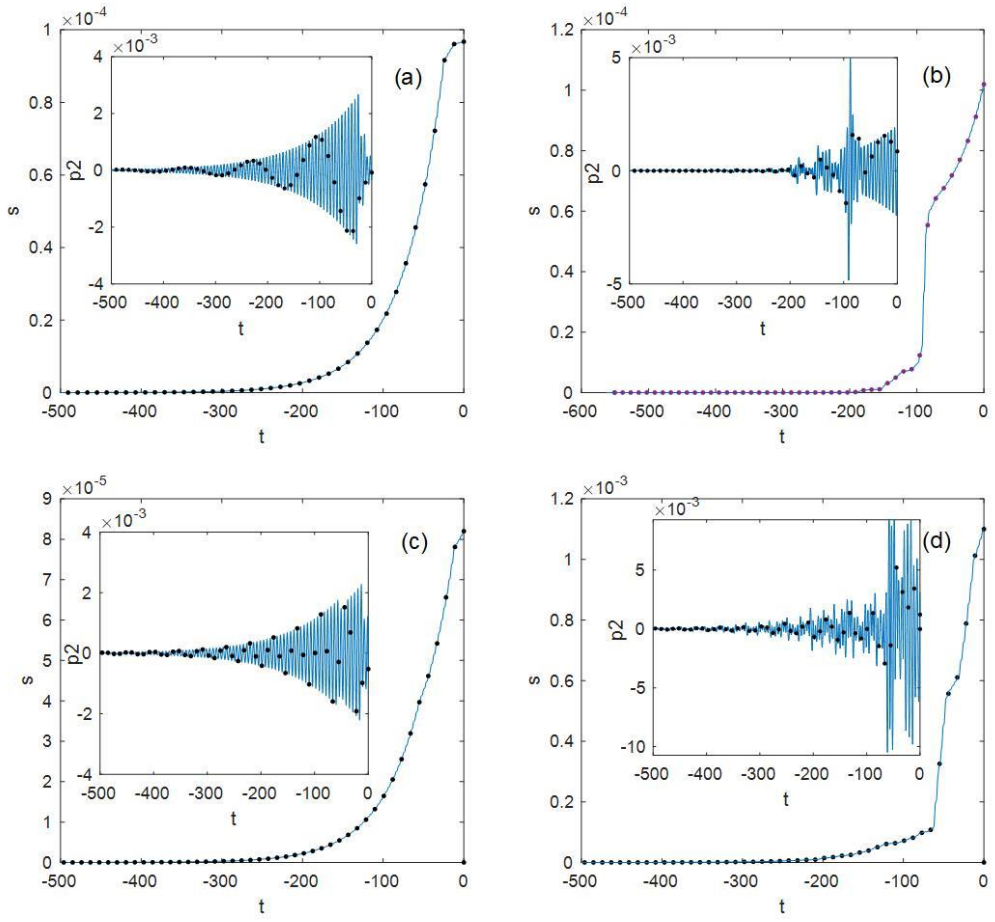

Fig.5 The time histories of the momentum p_2 and action s. The points are corresponding to the values in the Poincare section. (a) $\omega = 0.525$, attractor N. (b) $\omega = 0.525$, attractor I. (a) $\omega = 0.57$, attractor N. (b) $\omega = 0.57$, attractor I.

4. Numerical simulation

In the following, two numerical methods are applied to verify the above section's theoretical results. One is to obtain the system's stationary probability distribution by numerical simulation first, then by converting the stationary probability distribution according to the WKB approximation[43] to derive the global quasi-potential of the system. Another is to examine the MFETs for each attractor, then, according to the Arrhenius-type law [23] to determine each attractors' activation energies.

4.1 The Probability Distribution

Traditionally, the solution of the stationary probability distribution function is the main task for the stochastic system. However, for the complexity of the stochastic system, very few PDFs can be derived analytically. Even for the numerical Monte-Carlo simulation, the solution procedure is challenging and time-consuming. In this paper, the Stochastic Generalized Cell Mapping (SGCM) method[40] is applied. Rather than simulating the stochastic system for thousands of periods, we only need to simulate the system one period of time to derive the system's one-step transition probability matrix. Then, use the one-step transition probability matrix, the probability distribution of the system at any time could be calculated if the initial distribution is given.

Fig.6 shows a coup of probability densities of the displacement at different times with the initial

distribution given as a uniform distribution. As seen, the probability densities of the displacement derived by the SGCM method agreed well with the MC method. Moreover, Fig.7 gives the stationary joint probability density of velocity and displacement derived by the SGCM method. For both the parameters, the probabilities mainly focus on attractor I, especially for $\omega = 0.57$, the stationary probability is almost all absorbed by attractor I.

As we have seen, thorough observing the probability distribution can help us evaluate the attractors' stabilities, but it is a vague understanding. Actually, with the probability distribution in hand, we can give a piece of much more intuitive information about the system's stability than directly observe the probability distribution with a simple transformation. In the weak noise limit, the probability is entirely defined by the quasi-potential Ψ and is of Boltzmann form [25,38]

$$\Psi(x, y) \approx -D \ln p(x, y). \tag{25}$$

Moreover, the quasi-potential difference between the saddle and the attractor is the activation energy used to depict the attractor's stability. Therefore, by converting the stationary probability distribution derived above according to Eq.(25), we can approximately present the system's global quasi-potential.

Fig.8 shows the approximated global quasi-potential for both parameters. The higher the difference between the attractor and saddle is, the more stable the attractor is. For $\omega = 0.525$, the quasi-potential differences for attractor I and attractor N are 0.0000965 and 0.0000911, respectively. And for $\omega = 0.57$, the quasi-potential differences for attractor I and attractor N are 0.00109 and 0.000073. We can see they agree with the theoretical results derived in the above section well.

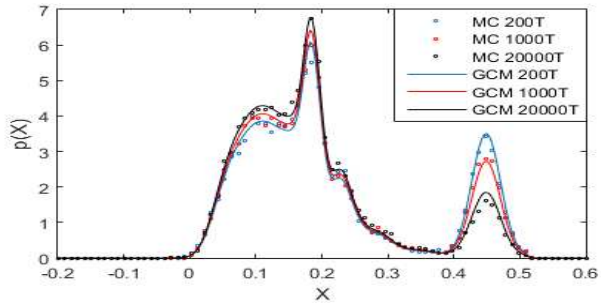

(a)

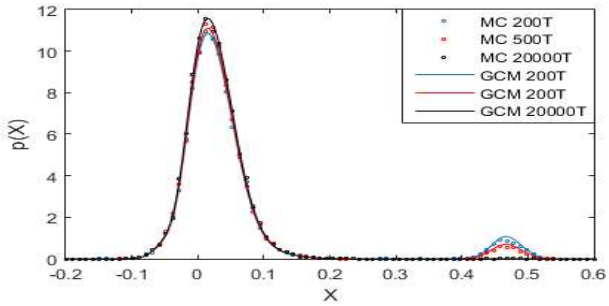

(b)

Fig.6 The displacement densities with the noise intensity $D = 0.00002$, the dotted lines are the results derived by the MC method, and the solid lines the results derived by the SGCM method. (a) $\omega = 0.525$,(b) $\omega = 0.57$

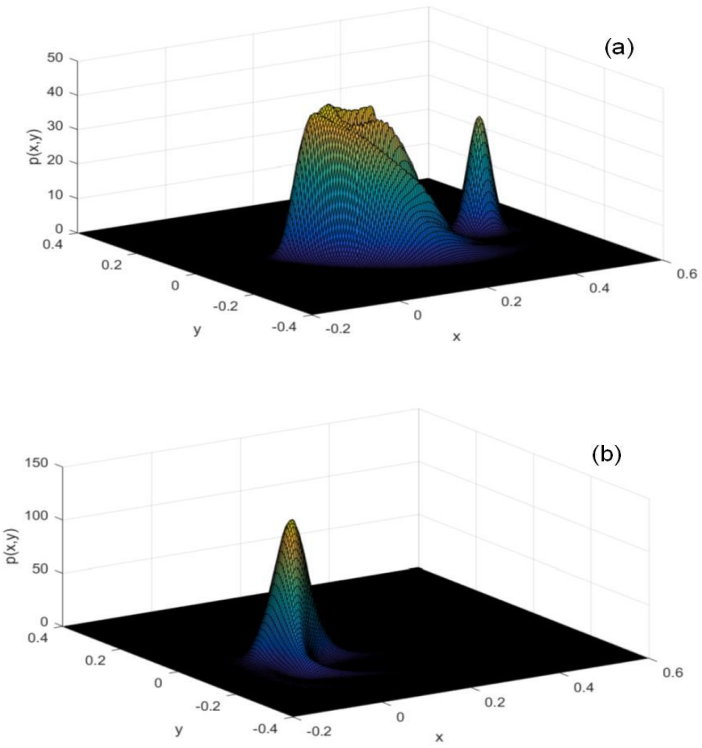

Fig.7 The stationary joint probability density of velocity and displacement derived by SGCM method with $D = 0.00002$. (a) $\omega = 0.525$,(b) $\omega = 0.57$

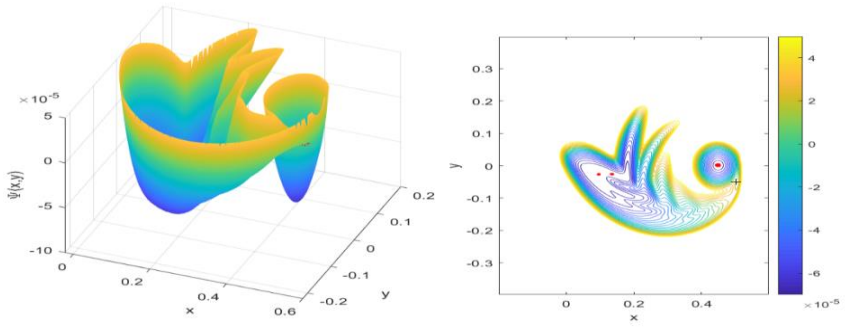

(a)

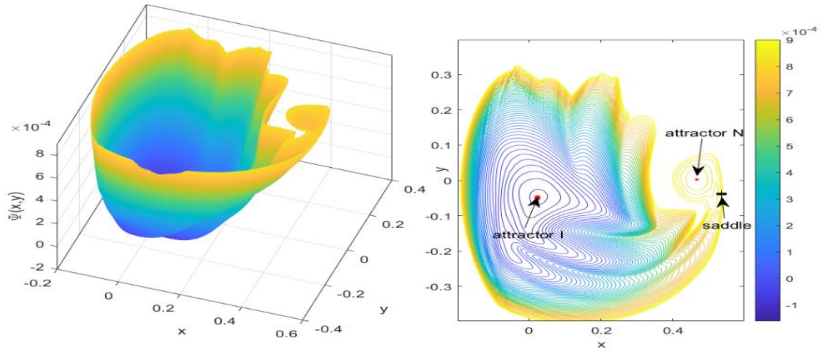

(b)

Fig.8 The global quasi-potential derived from the stationary probability densities. (a) $\omega = 0.525$,(b) $\omega = 0.57$.

4.2 Mean First Exit Time

The MFET is another critical quantity to measure the attractor's stability, its ability to survive random perturbations. In the weak noise limit $D \to 0$, the MFET is usually found to obey the Arrhenius law, which Kramer firstly obtained governing the potential system's transition rates in reaction kinetics[22].

$$\langle \tau_D \rangle \sim \exp(\Delta U / D). \tag{26}$$

ΔU plays the role of the activation energy or the height of potential well needed to escape from one attractor to another.

Several sets of MFET derived from the numerical MC simulation are shown in Fig.9. By fitting the data according to the equation(26), the activation energies for each attractor are estimated: for $\omega = 0.525$, the value of the activation energy $\Delta U_{\mathrm{I}} = 0.000114$ is found for attractor I and $\Delta U_{\mathrm{N}} = 0.000107$ for attractor N; for $\omega = 0.57$, the activation energies of attractor I and N are $\Delta U_{\mathrm{I}} = 0.001147$ and $\Delta U_{\mathrm{N}} = 0.000082$ respectively. We can see the results also agree well with the theoretical results.

Accompanied by the MFET, there is another essential quantity, the transition rate, which is inversely proportional to the MFET, and it has been shown of the form $W_D \sim \exp(-\Delta U / D)$ [27]. When the stochastic system attains a steady-state, the transitions between the attractors will reach a balance. For example, for the parameter $\omega = 0.57$, the transition rate W_D^{IN} from attractor I to attractor N equals approximately to $\exp(-0.001147/D)$, and the transition rate W_D^{NI} from attractor N to attractor I equals approximately $\exp(-0.000082/D)$. When the stochastic system reaches a steady-state, the transitions between the attractors will reach a balance $W_D^{\mathrm{IN}} P_{\mathrm{I}} = W_D^{\mathrm{NI}} P_{\mathrm{N}}$. Here P_{I} is the stationary probability around attractor I and P_{N} around attractor N. Due to $W_D^{\mathrm{IN}} \ll W_D^{\mathrm{NI}}$, P_{I} must be much greater than P_{N} to reach the steady-state, resulting in the high probability around attractor I in Fig.7(b), almost 100%.

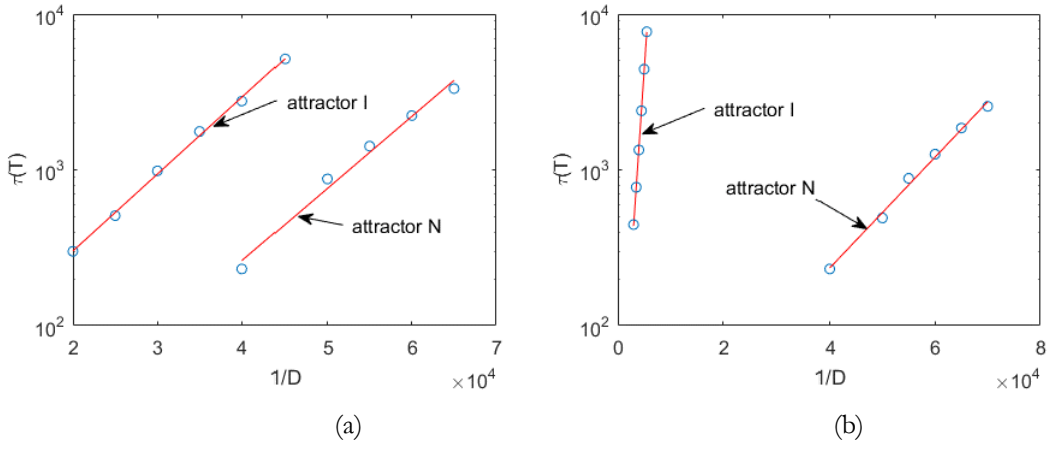

Fig.9 MFET versus the inverse of the noise intensity $1/D$. Each point is an average of τ_D over 1000 escape events obtained from stochastic simulation. (a): $\omega = 0.525$, (b): $\omega = 0.57$.

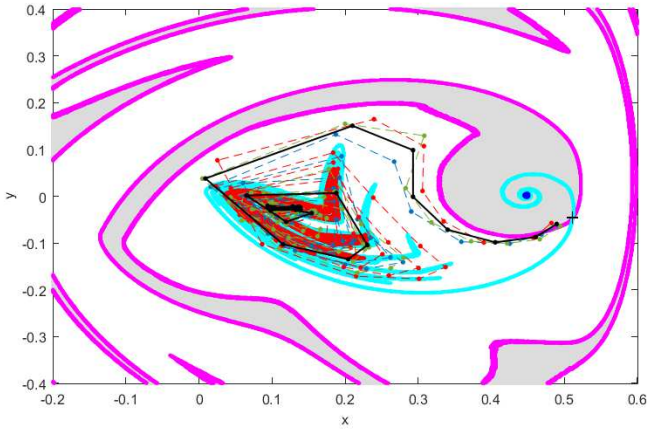

Fig.10 Some escape realizations for the attractor I under noise intensity $D = 0.000013$, $\omega = 0.525$ (The solid-line: the most probable exit path derived by the action plot. The dashed line: the escape realizations derived by MC method)

At last, for $\omega = 0.525$, several escape realizations before transiting into the domain of the attractor N are plotted in Fig.10. As is shown, when the particles leave the transition chaos, the escape realizations follow along the most probable exit path seemly in a deterministic way. However, in the transition chaos, due to its sensitivity to the noises, only when $D \to 0$ will the realizations move along the MPEP be observed.

5. Conclusion

In this paper, the stochastic stability of a Vibro-impact system is investigated. For the system excited by multiple external forces, including a constant force, a harmonic force, and a random perturbation, the PDF of the system is extremely difficult to solve. Moreover, considering the existence of multiple coexisting steady-states in the system and the random noise that will induce the transitions between the attractors, we have to work out each attractor's activation energy. Review from large deviation theory, the asymptotic analysis for our system in weak noise limit is carried out, and a time-varying Hamilton's equation for the quasi-potential is derived. To validate the effectiveness of theoretical analysis, two examples are tested, and the results show good agreement with the numerical simulation. Furthermore, an interesting phenomenon is observed. In both examples, a non-impact attractor and an impact attractor coexist together in the system, and the domains of attraction are very similar. From the size of the attraction domain, it should be judged that the stabilities of the impact attractors in both examples should be about the same order. However, the derived activation energies of the impact attractors show a very dramatic difference. That lies in, in one of the examples, a transient chaos existing near the impactor attractor in seriously reduced the effective attraction domain and made

the attractor much closer to the saddle point. Hence, in engineering, the common intuition to judge the stability from the size of the attraction domain is usually unreliable. A formal way is to follow our paper to have an asymptotic analysis for the system and determine each attractor's stability.

Acknowledgments

This research was supported by the National Natural Science Foundation of China (Grants 11772149), the Research Fund of State Key Laboratory of Mechanics and Control of Mechanical Structures (Nanjing University of Aeronautics and Astronautics) (Grant No. MCMS-I-19G01), and the Project Funded by the Priority Academic Program Development of Jiangsu Higher Education Institutions(PAPD).

Compliance with ethical standards

Conflict of interest The authors declare that they have no conflict of interest.

Reference

[1] R. a Ibrahim, Vibro-Impact Dynamics: Modeling, Mapping and Applications, 2009. https://doi.org/10.1007/978-3-642-33968-4.

[2] J. Xie, W. Ding, Hopf-Hopf bifurcation and invariant torus T2 of a vibro-impact system, Int. J. Non. Linear. Mech. 40 (2005) 531–543. https://doi.org/10.1016/j.ijnonlinmec.2004.07.015.

[3] D.J. Wagg, S.R. Bishop, Chatter, sticking and chaotic impacting motion in a two-degree of freedom impact oscillator, Int. J. Bifurc. Chaos. 11 (2001) 57–71. https://doi.org/10.1142/S0218127401001943.

[4] D.J. Wagg, Periodic sticking motion in a two-degree-of-freedom impact oscillator, Int. J. Non. Linear. Mech. 40 (2005) 1076–1087. https://doi.org/10.1016/j.ijnonlinmec.2005.03.002.

[5] Amine, Bichri, Mohamed, BelhaqJoël, Perret-Liaudet, Control of vibroimpact dynamics of a single-sided Hertzian contact forced oscillator, Nonlinear Dyn. 63 (2011) 51–60.

[6] Jose, Antunes, Vincent, Debut, Laurent, Borsoi, Xavier, Delaune, Philippe, Piteau, A modal Udwadia-Kalaba formulation for vibro-impact modelling of continuous flexible systems with intermittent contacts, Procedia Eng. 199 (2017) 322–329.

[7] R., R., Aguiar, H., I., Weber, Mathematical modeling and experimental investigation of an embedded vibro-impact system, Nonlinear Dyn. 65 (2011) 317–334.

[8] L.H. Xie, Hopf Bifurcation of a two-degree-of-freedom Vibr-impactT system, J. Sound Vib. 213 (1998) 391–408.

[9] Z.L. Huang, Z.H. Liu, W.Q. Zhu, Stationary response of multi-degree-of-freedom vibro-impact systems under white noise excitations, J. Sound Vib. 275 (2004) 223–240.

[10] C. Li, W. Xu, J. Feng, L. Wang, Response probability density functions of Duffing–Van der Pol vibro-impact system under correlated Gaussian white noise excitations, Phys. A Statal Mech. Its Appl. 392 (2013) 1269–1279.

[11] M.F. Dimentberg, A.I. Menyailov, Response of a Single - mass Vibroimpact System to White - noise Random Excitation, J. Appl. Math. Mech. 59 (2010) 709–716.

[12] Zhu, T. H., Stochastic response of a vibro-impact Duffing system under external Poisson

impulses, Nonlinear Dyn. 82 (2015) 1001–1013.

[13] J. Feng, W. Xu, R. Wang, Stochastic responses of vibro-impact duffing oscillator excited by additive Gaussian noise, J. Sound Vib. 309 (2008) 730–738. https://doi.org/10.1016/j.jsv.2007.07.070.

[14] J. Feng, W. Xu, H. Rong, R. Wang, Stochastic responses of Duffing-Van der Pol vibro-impact system under additive and multiplicative random excitations, Int. J. Non. Linear. Mech. 44 (2009) 51–57. https://doi.org/10.1016/j.ijnonlinmec.2008.08.013.

[15] C. Li, W. Xu, L. Wang, D.X. Li, Stochastic responses of Duffing - Van der Pol vibro-impact system under additive colored noise excitation, Chinese Phys. B. 11 (2013) 159–165. https://doi.org/10.1088/1674-1056/22/11/110205.

[16] Y. Wu, W.Q. Zhu, Stationary response of multi-degree-of-freedom vibro-impact systems to Poisson white noises, Phys. Lett. A. 372 (2008) 623–630. https://doi.org/10.1016/j.physleta.2007.07.083.

[17] W. Xu, C. Li, X. Yue, H. Rong, Stochastic responses of a vibro-impact system with additive and multiplicative colored noise excitations, Int. J. Dyn. Control. 4 (2016) 393–399. https://doi.org/10.1007/s40435-014-0143-0.

[18] M.F. Dimentberg, O. Gaidai, A. Naess, Random vibrations with strongly inelastic impacts: Response PDF by the path integration method, Int. J. Non. Linear. Mech. 44 (2009) 791–796. https://doi.org/10.1016/j.ijnonlinmec.2009.04.007.

[19] R.S. Maier, D.L. Stein, Limiting exit location distributions in the stochastic exit problem, SIAM J. Appl. Math. 57 (1997) 752–790.

[20] P.D. Beale, Noise-induced escape from attractors, Phys. Rev. A. 22 (1989) 3283.

[21] D'Onofrio, Alberto, Bounded-noise-induced transitions in a tumor-immune system interplay, Phys. Rev. E. 81 (2010) 21923.

[22] H.A. Kramers, Brownian motion in a field of force and the diffusion model of chemical reactions, Physica. 7 (1940) 284–304. https://doi.org/10.1016/S0031-8914(40)90098-2.

[23] H.A. Kramers, Brownian motion in a field of force and the diffusion model of chemical reaction, Physica. 7 (1940) 284–304.

[24] Z. Schuss, Theory and Applications of Stochastic Differential Equations, Phys. Today. 34 (1981) 95–97.

[25] M. Freidlin, A.D. Wentzell, Random Perturbations of Dynamical Systems, Springer New York, 1988.

[26] J.Q. Feng, T. Wang, W. Xu, The Noise-Induced Chaotic Transition in a Vibro-Impact Oscillator, Appl. Mech. Mater. 117–119 (2012) 347–350. https://doi.org/10.4028/www.scientific.net/AMM.117-119.347.

[27] R.V. Roy, Global stability analysis of nonlinear dynamic systems.Series on Stability, Vib. Control Syst. Ser. B. 9 (1997) 261–295.

[28] S. Beri, R. Mannella, D.G. Luchinsky, A.N. Silchenko, P.V.E. Mcclintock, Solution of the boundary value problem for optimal escape in continuous stochastic systems and maps, Phys. Rev. E. (2005) 1–16. https://doi.org/10.1103/PhysRevE.72.036131.

[29] R.J. Comparin, R. Singh, Non-linear frequency response characteristics of an impact pair, J. Sound Vib. 134 (2015) 259–290.

[30] P.J. Holmes, The dynamics of repeated impacts with a sinusoidally vibrating table, J. Sound Vib. 84 (1982) 173–189.

[31] C.N. Bapat, C. Bapat, Impact-pair under periodic excitation, J. Sound Vib. 120 (1988) 53–61.

[32] M.S. Heiman, P.J. Sherman, A.K. Bajaj, On the dynamics and stability of an inclined impact pair, J. Sound Vib. 114 (1987) 535–547.

[33] R. V Roy, E. Nauman, Noise-induced effects on a non-linear oscillator, J. Sound Vib. 183 (1995) 269–295.

[34] R.V. Roy, Global stability analysis of nonlinear dynamic systems, Ser. Stab., Vib. Control Syst. Ser. B (1997) 261–295.

[35] Z.L. Huang, Z.H. Liu, W.Q. Zhu, Stationary response of multi-degree-of-freedom vibro-impact systems under white noise excitations, J. Sound Vib. 275 (2004) 223–240. https://doi.org/10.1016/j.jsv.2003.06.007.

[36] D.P. Hess, A. Soom, C.H. Kim, Normal vibrations and friction at a Hertzian contact under random excitation: Theory and experiments, J. Sound Vib. 153 (1992) 491–508. https://doi.org/https://doi.org/10.1016/0022-460X(92)90378-B.

[37] R.V. Roy, Averaging method for strongly non-linear oscillators with periodic excitations, Int. J. Non. Linear. Mech. 29 (1994) 737–753. https://doi.org/10.1016/0020-7462(94)90068-X.

[38] R. Graham, T. Tél, Weak-noise limit of Fokker-Planck models and nondifferentiable potentials for dissipative dynamical systems, Phys. Rev. A. 31 (1985) 1109–1122.

[39] S.J. Einchcomb, A.J. Mckane, Use of Hamiltonian mechanics in systems driven by colored noise, Phys. Rev. E Stat. Phys. Plasmas Fluids Relat. Interdiscip. Top. 51 (1995) 2974–2981.

[40] C.S. Hsu, H.M. Chiu, A cell mapping method for nonlinear deterministic and stochastic systems. I. The method of analysis., J. Appl. Mech. 53 (1986) 695–701.

[41] S. Kraut, U. Feudel, Noise-induced escape through a chaotic saddle : lowering of the activation energy, Phys. D Nonlinear Phenom. 181 (2003) 222–234. https://doi.org/10.1016/S0167-2789(03)00098-8.

[42] L. Serdukova, Y. Zheng, J. Duan, J. Kurths, Stochastic basins of attraction for metastable states, Chaos. 26 (2016) 327–356.

[43] Z. Chen, X. Liu, Patterns and singular features of extreme fluctuational paths of a periodically driven system, Phys. Lett. A. 380 (2016) 1953–1958. https://doi.org/10.1016/j.physleta.2016.04.004.

Figures

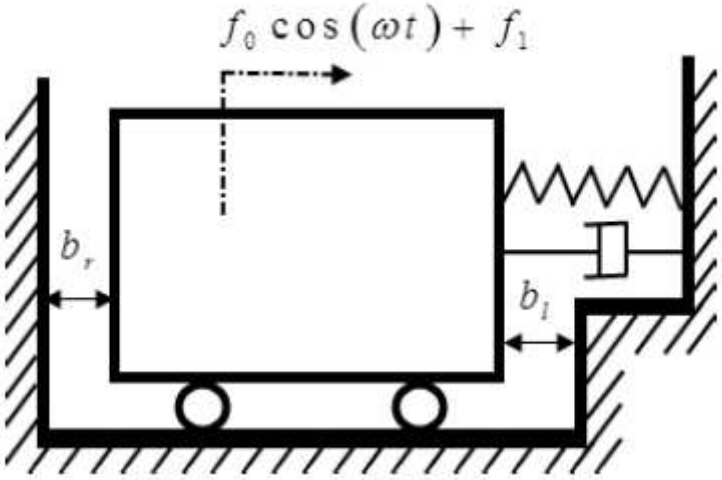

Figure 1

Schematic model of Vibro-impact oscillator

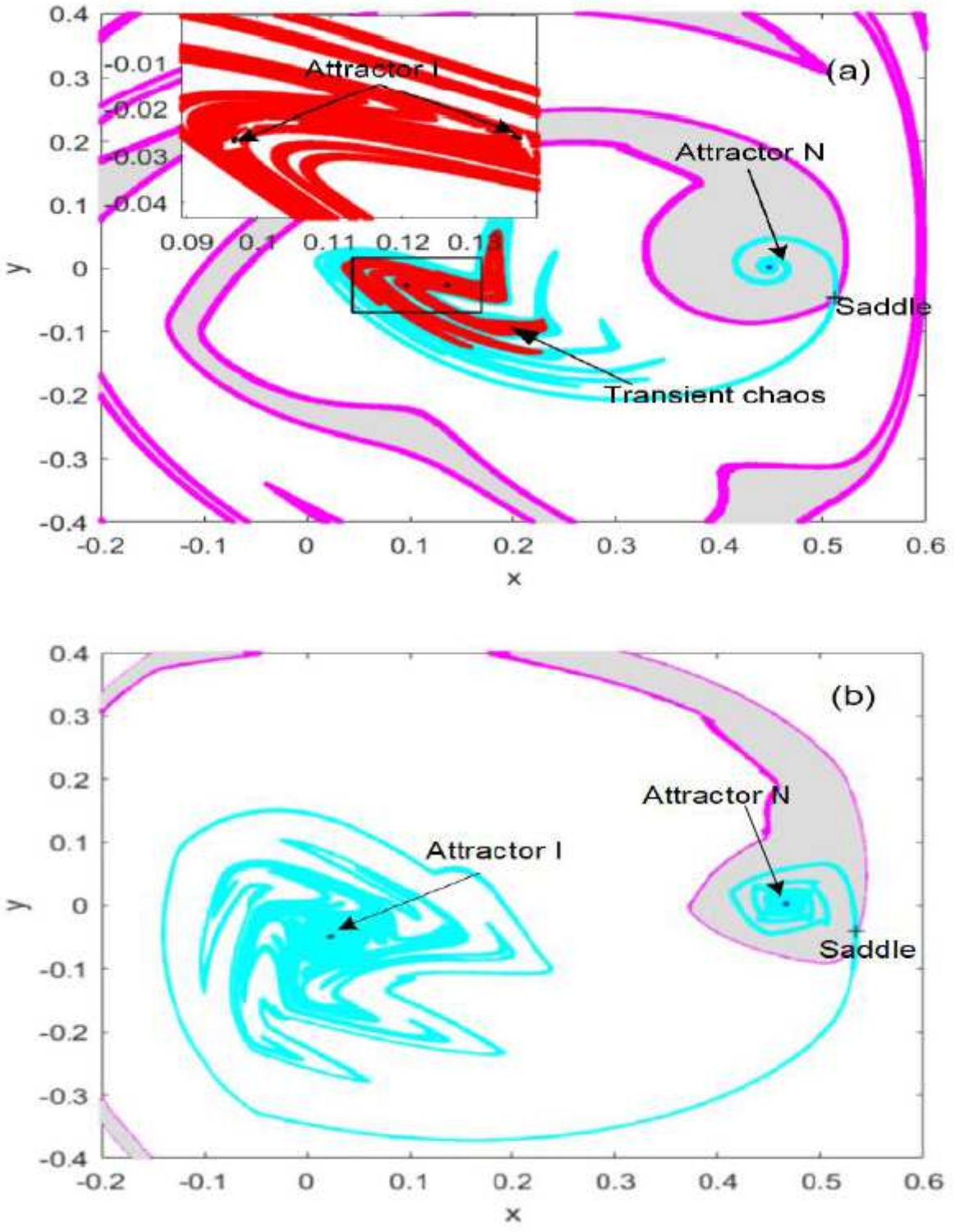

Figure 2

Vibro-impact system's global structure on the Poincare section: attractors, semi-attractors, stable and unstable manifolds of the semi-attractors. (a) ω = 0.525 ,(b) ω = 0.570

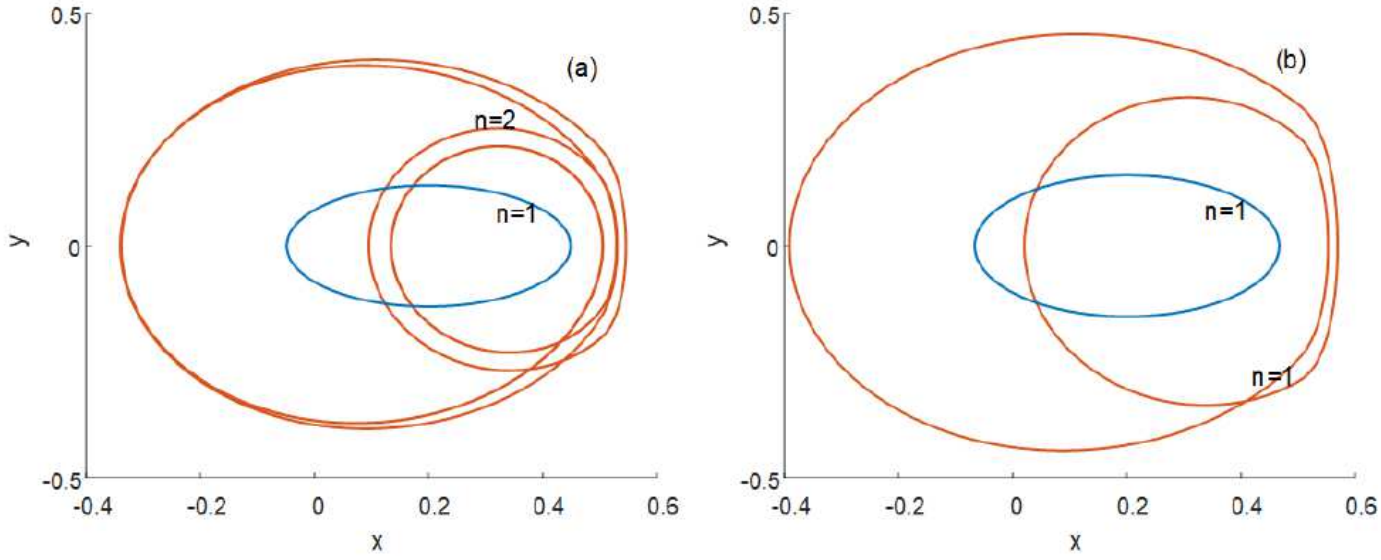

Figure 3

The steady-state phase projection: (a) ω = 0.525 : a steady periodic two impact orbit coexists with a periodic one non-impact orbit. (b) ω = 0.570 : a steady periodic one impact orbit, a steady periodic one non-impact orbit.

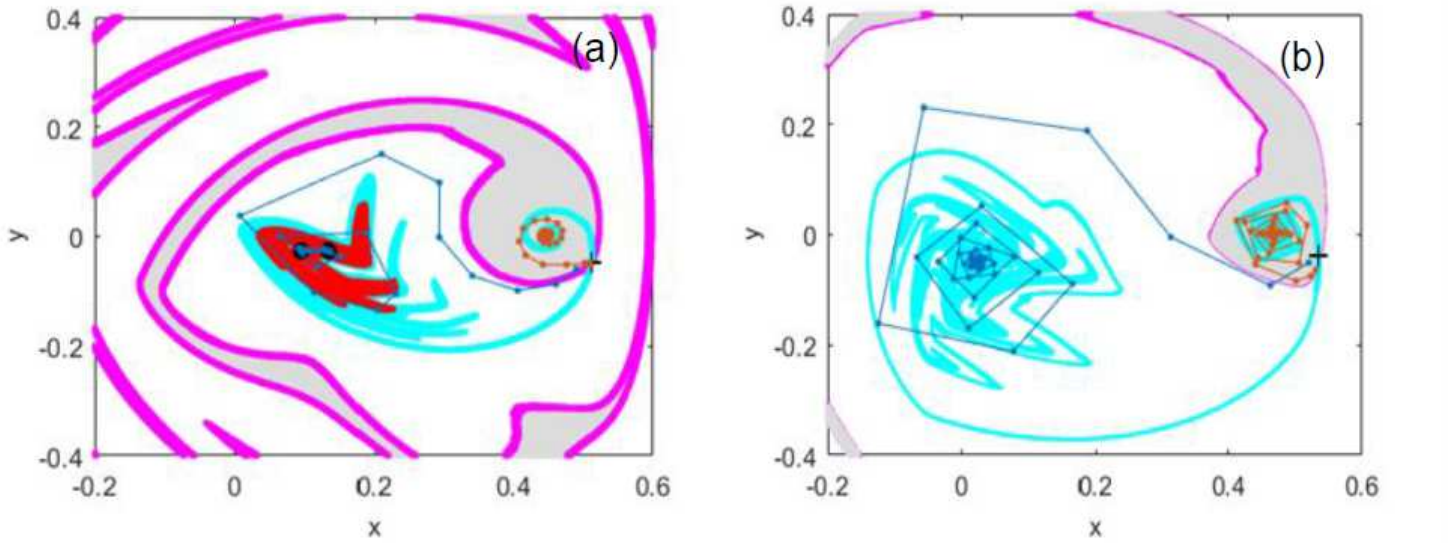

Figure 4

The MPEPs derived by the action plot. The dark blue dash lines are the most probable exit paths exiting from attractor I, and the brown ones are the most probable exit paths exiting from attractor N. (a) ω = 0.525 ,(b) ω = 0.57.

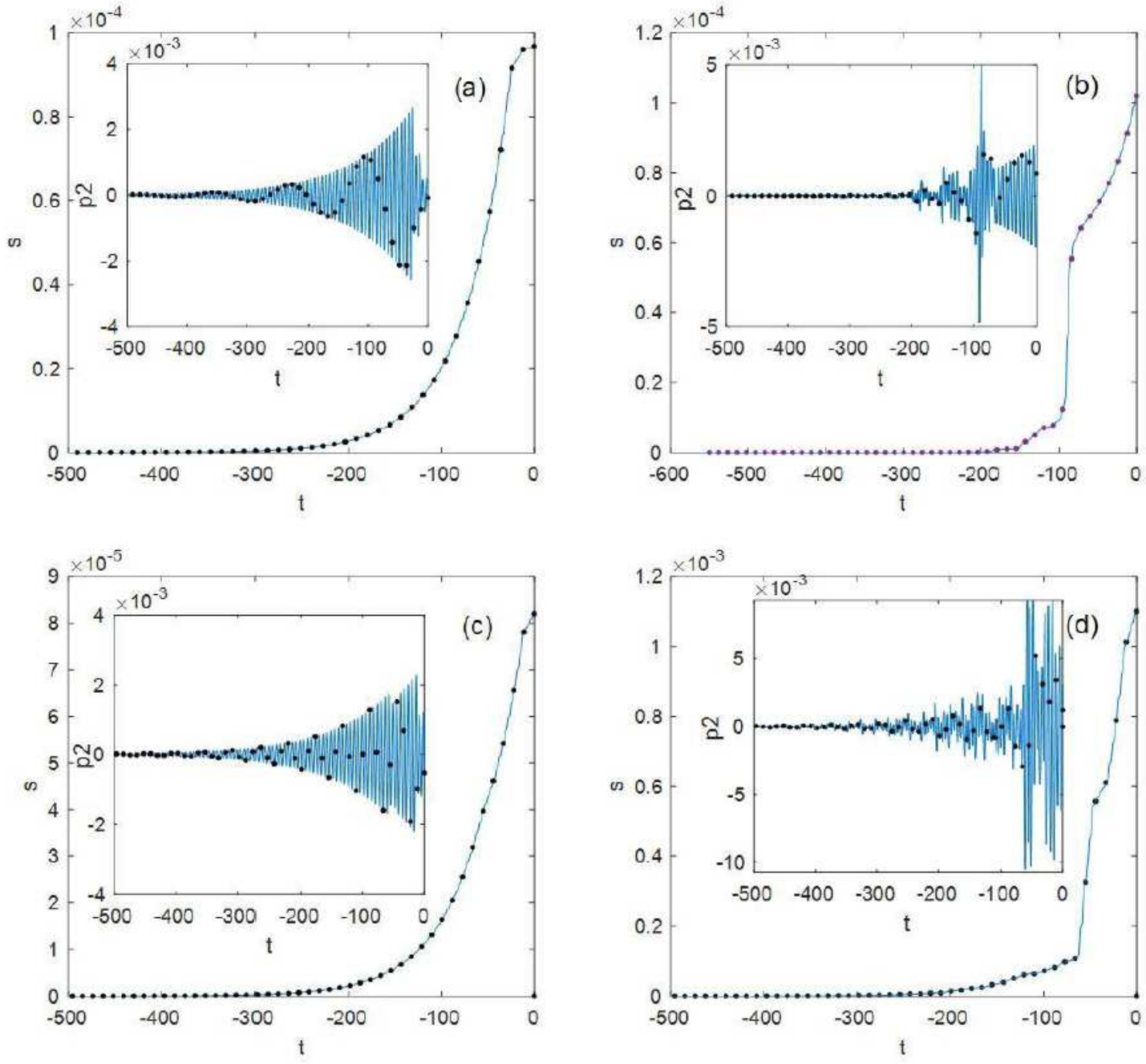

Figure 5

The time histories of the momentum p2 and action s . The points are corresponding to the values in the Poincare section. (a) ω = 0.525 , attractor N. (b)ω = 0.525 , attractor I. (a) ω = 0.57 , attractor N. (b) ω = 0.57 , attractor I.

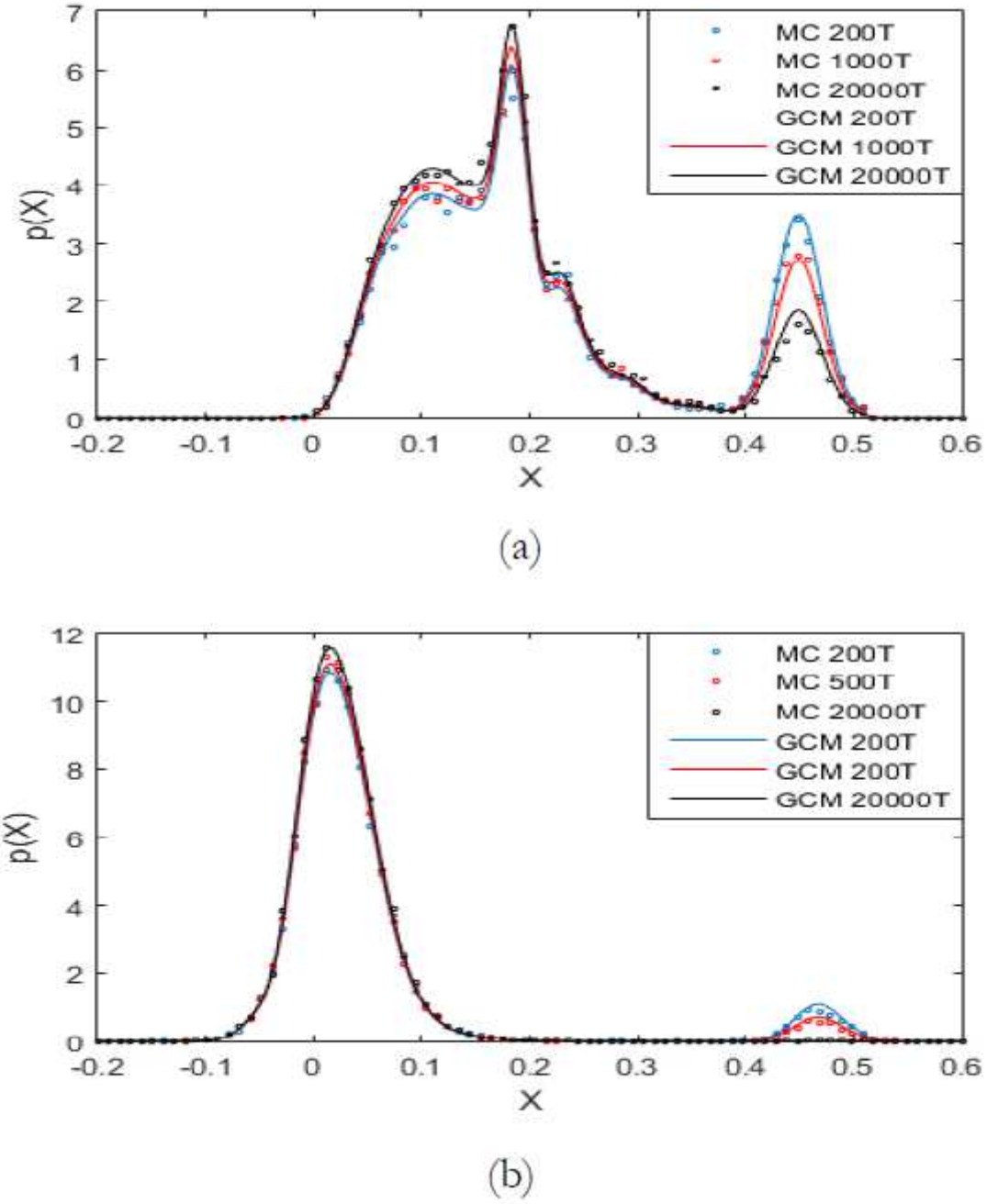

Figure 6

The displacement densities with the noise intensity D = 0.00002 , the dotted lines are the results derived by the MC method, and the solid lines the results derived by the SGCM method. (a) ω = 0.525 ,(b) ω = 0.57

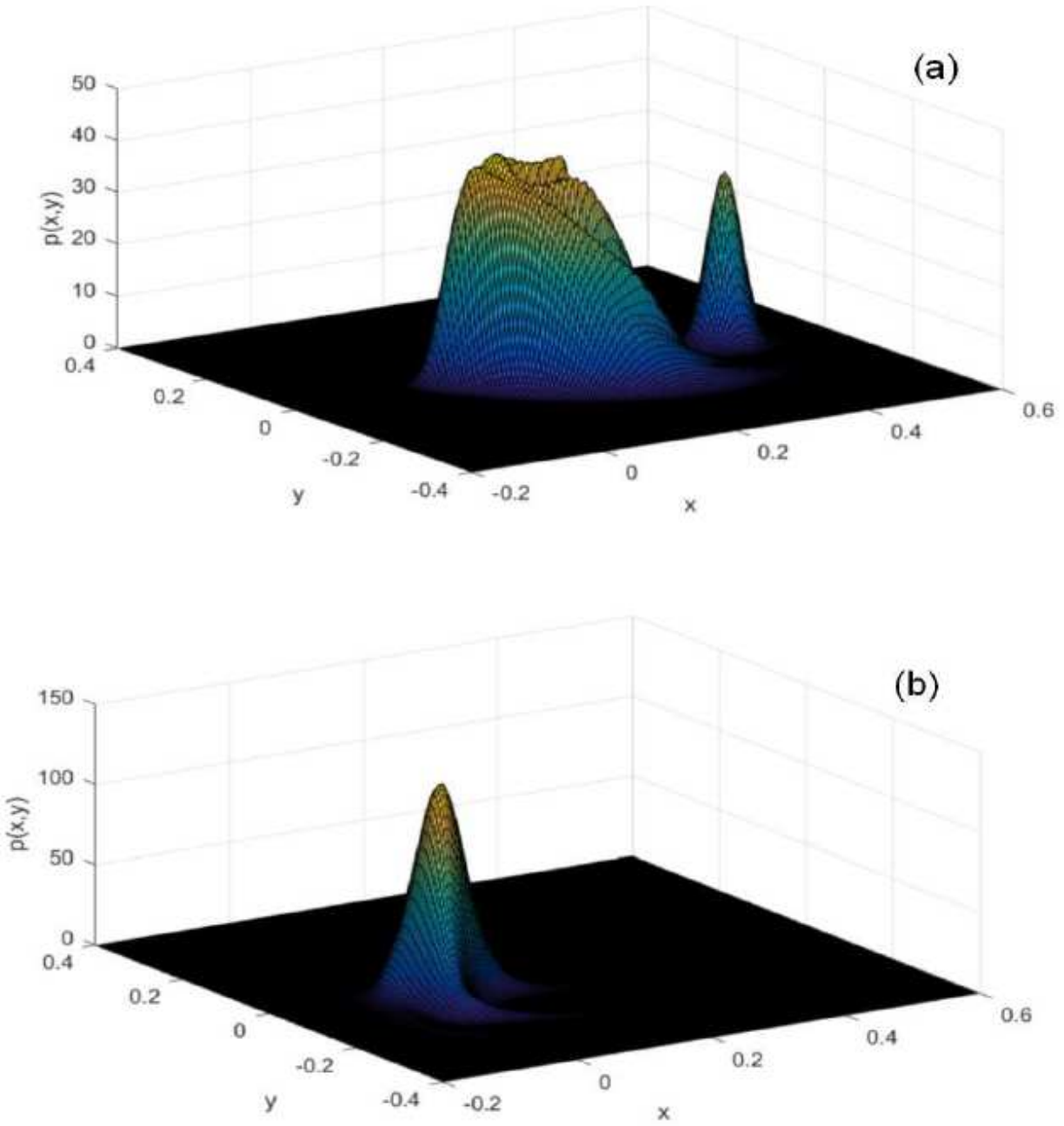

Figure 7

The stationary joint probability density of velocity and displacement derived by SGCM method with D = 0.00002 . (a) ω = 0.525 ,(b) ω = 0.57

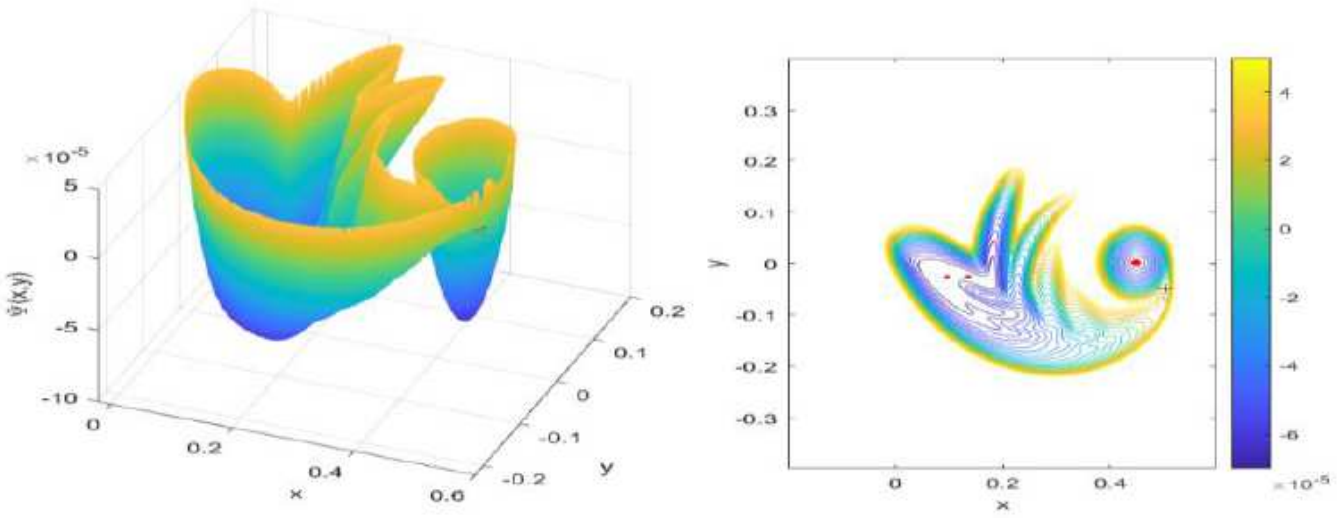

(a)

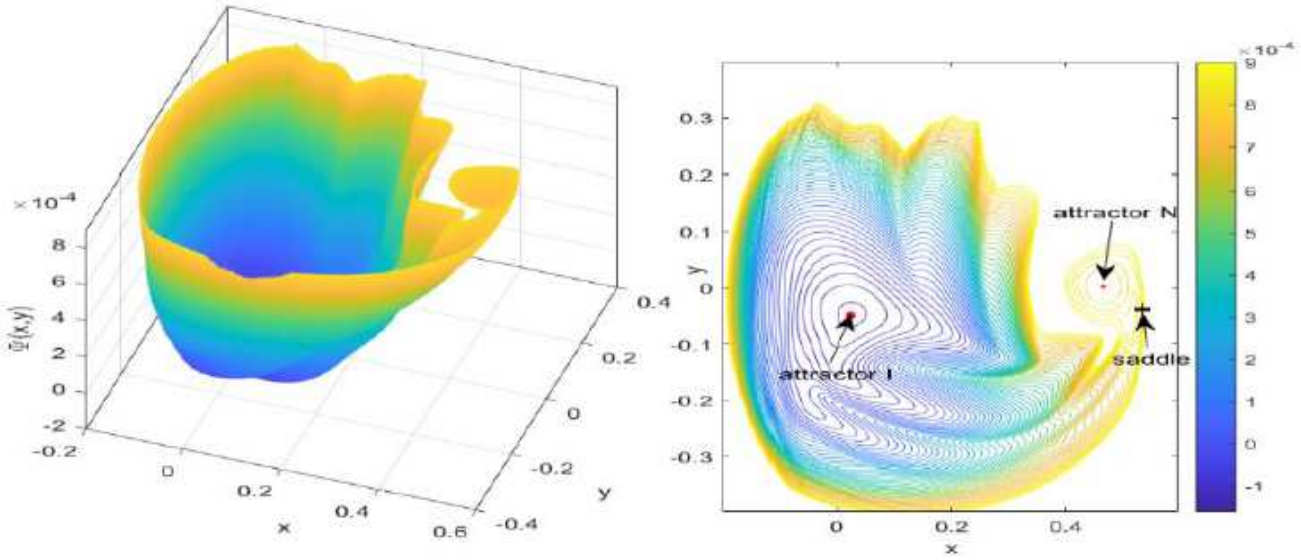

(b)

Figure 8

The global quasi-potential derived from the stationary probability densities. (a) ω = 0.525 ,(b) ω = 0.57 .

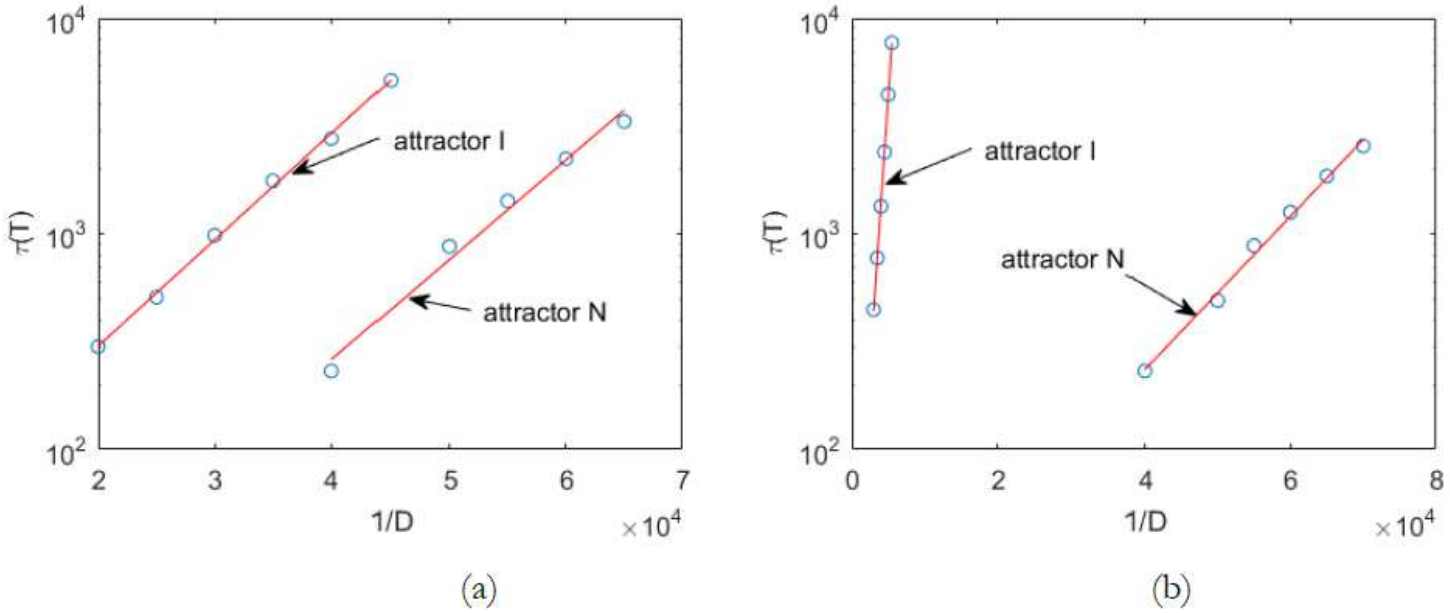

Figure 9

MFET versus the inverse of the noise intensity1/D . Each point is an average of τD = over 1000 escape events obtained from stochastic simulation. (a): ω = 0.525 , (b): ω =0.57 .

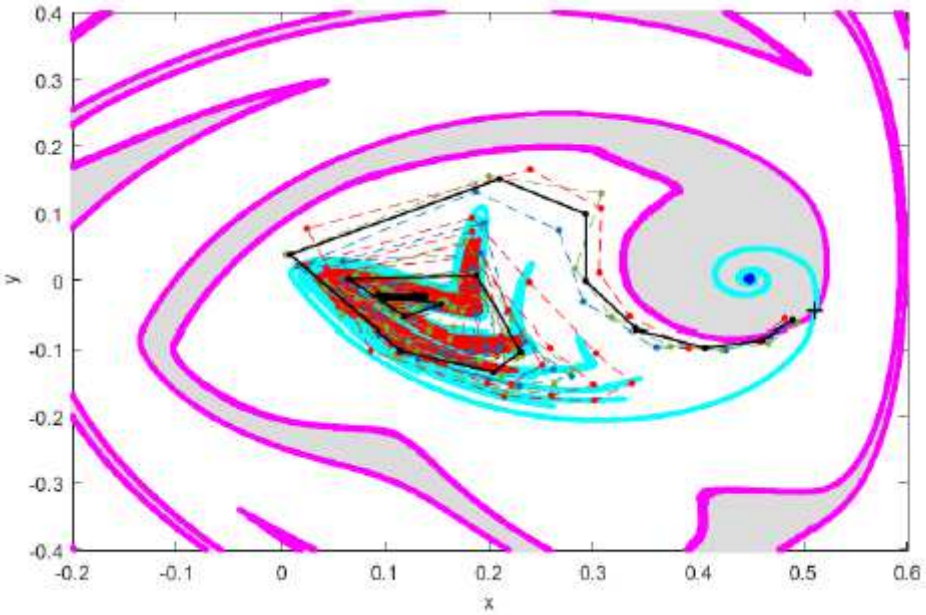

Figure 10

Some escape realizations for the attractor I under noise intensity D =0.000013 , ω = 0.525 (The solid-line: the most probable exit path derived by the action plot. The dashed line: the escape realizations derived by MC method